

Essential Spaces Defined by NMR Structure Ensembles and Molecular Dynamics Simulation Show Significant Overlap

Roger Abseher,¹ Lennard Horstink,² Cornelis W. Hilbers,² and Michael Nilges^{1*}

¹European Molecular Biology Laboratory, Heidelberg, Germany

²NSR Center, Laboratory of Biophysical Chemistry, University of Nijmegen, Nijmegen, The Netherlands

ABSTRACT Large concerted motions of proteins which span its “essential space,” are an important component of protein dynamics. We investigate to what extent structure ensembles generated with standard structure calculation techniques such as simulated annealing can capture these motions by comparing them to long-time molecular dynamics (MD) trajectories. The motions are analyzed by principal component analysis and compared using inner products of eigenvectors of the respective covariance matrices. Two very different systems are studied, the β -spectrin PH domain and the single-stranded DNA binding protein (ssDBP) from the filamentous phage Pf3. A comparison of the ensembles from NMR and MD shows significant overlap of the essential spaces, which in the case of ssDBP is extraordinarily high. The influence of variations in the specifications of distance restraints is investigated. We also study the influence of the selection criterion for the final structure ensemble on the definition of mobility. The results suggest a modified criterion that improves conformational sampling in terms of amplitudes of correlated motion. *Proteins* 31:370–382, 1998.

© 1998 Wiley-Liss, Inc.

Key words: NMR structure refinement; correlated/collective motion; essential dynamics analysis; PH domain; single-stranded DNA binding protein; gene V protein

INTRODUCTION

Solution structures of biomolecules solved by nuclear magnetic resonance (NMR) spectroscopy are usually reported as ensembles of structures fulfilling the experimental restraints to a similar and high extent. The dynamic information implicitly present in NOE data is qualitatively expressed via loose distance bounds. Therefore, we may hope that ensembles of NMR structures tell something about internal dynamics. Simply equating local diversity of structures to motion may be misleading, however, since it may be a consequence of missing data.

Independently obtained data are required for validation. NMR spectroscopy itself is a valuable source of independent dynamic data apt for validation. Comparison of squared order parameters obtained from the analysis of ¹⁵N relaxation data to the global backbone RMSD per residue was recently used not only for validation, but also as a criterion for which structures are to be included in a complete and consistent representation of the solution structure of ribonuclease T₁.¹ A shortcoming of heteronuclear relaxation data is that they may fail to detect large-scale correlated motion. This is mainly due to: (1) The timescale of large-scale correlated motion is frequently too slow to be fully detected by relaxation measurements, which are sensitive to mobility on a picosecond and nanosecond timescale. Slower motions only show up in the transverse relaxation time T₂, but not in the other parameters. (2) Certain correlated motions, such as a sliding motion of a secondary structure element with respect to the rest of the molecule, do not alter the orientation of an N–H or C–H vector significantly with respect to a molecule-fixed axis. Furthermore, it is not possible to distinguish between correlated and uncorrelated motion of two X–H vectors by standard relaxation measurements. As correlated motion may be relevant for biological function, these shortcomings are significant.

Molecular dynamics (MD) simulation is a source of detailed information on mobility. However, it suffers from a simplified, approximate description of interactions and is currently limited to a nanosecond timescale. In contrast to NMR relaxation measurements, the latter is not a principal limitation. It is surmount-

Abbreviations: NMR, nuclear magnetic resonance; NOE, nuclear Overhauser effect; MD, molecular dynamics; PH domain, pleckstrin homology domain; ssDBP, single-stranded DNA binding protein; DBW, DNA binding wing in ssDBP; DL, dyad loop in ssDBP; CL, complex loop in ssDBP; BPTI, bovine pancreatic trypsin inhibitor; RMSD, root mean square deviation; ACSIP, average cumulative square inner product.

Grant sponsor: The Supercomputing Resource for Molecular Biology at the European Molecular Biology Laboratory, funded by a European Union Human Capital and Mobility Access to Large Scale Facilities; Grant number: ERBCHGECT940062.

*Correspondence to: Michael Nilges, Meyerhofstraße 1, D-69117 Heidelberg, Germany. E-mail: nilges@embl-heidelberg.de

able by increased computing power. At the same time, the observation of nanosecond timescale motion even in a 500 ps trajectory is not a problem of sensitivity, but rather a statistical problem. MD simulations were successfully used previously for describing fast local internal motion in the refinement of the solution structure of a DNA octamer.² Squared order parameters calculated from an MD trajectory significantly improved the agreement between simulated and experimental 2D NOESY spectra in an approach that accounts for both spin diffusion and internal dynamics. Similarly, a recent comparison of families of structures comprising snapshots taken at regular intervals from MD trajectories with NMR structure ensembles of BPTI by visual inspection and in terms of RMSDs revealed significant overlap.³ A salient feature of MD simulation is that it provides direct access to the correlated motions on the timescale sampled by a given trajectory. Modes derived from a reliable trajectory may even allow extrapolation to a somewhat longer timescale than that of the trajectory itself.⁴ The essential dynamics analysis method⁵ performs a decomposition of internal motions into modes and sorts them according to their amplitudes. The modes and amplitudes are calculated as eigenvectors and eigenvalues of a covariance matrix⁶ containing all information about correlated displacements of atoms. Rather few modes—those with the largest amplitudes—account for a high percentage of the total mobility observed.^{5,7} Biofunctionally important motions are observed to occur among these so-called “essential modes.”^{7,8,9}

The essential dynamics analysis is applicable not only to MD trajectories but to any series of coordinate frames of a system, e.g., an NMR structure ensemble.⁷ The diversity of NMR structure ensembles is then translated into modes of correlated motion. As an ensemble of NMR structures is not a series of frames ordered in time, no information about timescales can be expected from such an analysis. Therefore, the study focuses on directions in conformational space and associated amplitudes. This allows for an assessment of the capability of NMR structure ensembles to capture correlated motion. If such ensembles described the large-scale motions of a protein in a similar way as MD simulations do, it would be both surprising and valuable. Surprising because MD and NMR structure calculations employ different force fields and methods of conformational search; valuable because it would offer a shortcut to the characterization of biofunctionally important motion. In the present study, the essential dynamics analysis is applied to both NMR structure ensembles and long-time MD trajectories of two very different proteins, the β -spectrin pleckstrin homology domain (PH domain), a globular protein with flexible surface loops,^{10,11} and the single-

stranded DNA binding protein (ssDBP) from bacteriophage Pf3,¹² a homodimeric protein with DNA binding wings protruding far from the core of the molecule. As MD trajectories are used here as a reference for judging the definition of correlated motion given by NMR structure ensembles, particular care has to be taken to ensure their reliability. In the case of the PH domain, different simulation methods and different starting structures were used; all yield significantly overlapping definitions of the essential space, which is the part of the configurational space spanned by the essential modes.

It was shown previously that distance restraining, as performed during NMR structure calculation, inhibits the motion in the essential subspace.¹³ Amplitudes of fluctuations were compared between free MD simulations and MD with time-averaged restraints. Marked differences in the amplitudes of the first few eigenvectors were reported, i.e., lower amplitudes for the simulation with restraints. The restraints used in the standard structure calculation approach are even more stringent than time-averaged restraints, since they are static, i.e., they have to be fulfilled by each structure at any time, not only on average. In addition, only a fraction of all structures (those with few violations) are reported. At the same time, there are indications that the range of conformations available to proteins at ambient temperature may be even larger than usually expected.¹⁴ The range of conformations available to a biomolecule is relevant for the understanding of many intermolecular interactions that are not fully explained in terms of a key-in-lock fitting, but rather involve mutual adjustments of the structures in the process of binding. In this study, we suggest a new cutoff criterion for the definition of a solution structure ensemble that does not underestimate mobility.

SYSTEMS AND METHODS

Systems

The β -spectrin PH domain is a 106 residue protein module. The two longest loops (between β -sheets $\beta 1$ and $\beta 2$ and between $\beta 5$ and $\beta 6$, cf. Fig. 1) have a high content of basic residues and provide the binding pocket for the inositol phosphate ligand,¹⁵ which is negatively charged under physiological conditions.

The ssDBP protein is a C_2 -symmetric homodimer. Each monomer consists of seven β -strands, of which five strands form a five-stranded antiparallel sheet making up the core of the molecule. Two β -hairpins and a loop protrude from this core and are involved in the function of ssDBP: residues 11–25 are referred to as “DNA binding wing,” 31–36 as “complex loop,” and 51–70 as “dyad loop”¹² (cf. Fig. 1). The dyad loop makes up the interface between two monomers within a dimer and the complex loop provides the interface for the interaction between dimers in a super-helical assembly, which is formed in a highly cooperative manner upon binding single-stranded

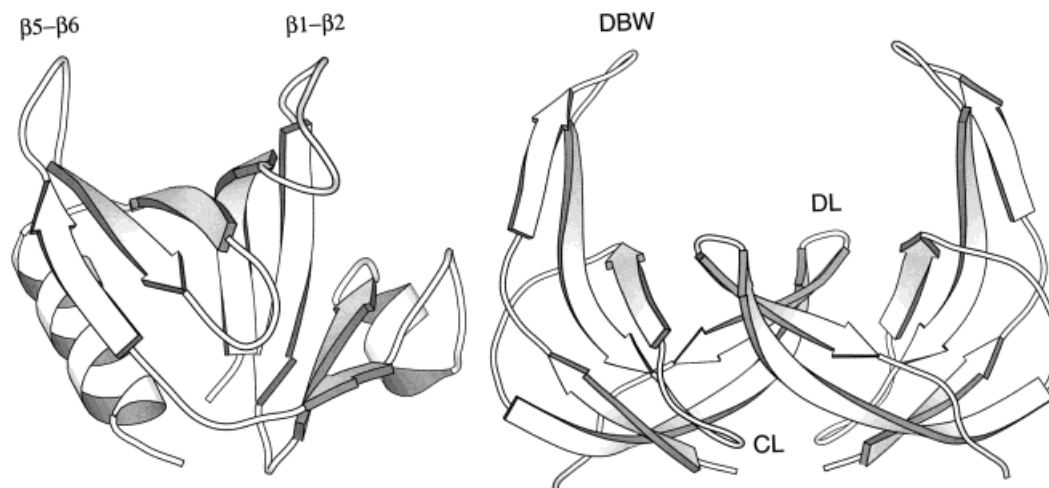


Fig. 1. Molscript³³ pictures of the PH domain (left) and the ssDBP protein (right). The ligand binding loops ($\beta 1$ – $\beta 2$, $\beta 5$ – $\beta 6$) in the PH domain as well as the DNA binding wing (DBW), the dyad loop (DL), and the complex loop (CL) in one chain of ssDBP are indicated.

DNA. The assembly was modeled by restrained molecular dynamics based on electron microscopy data for the highly homologous gene V protein from bacteriophage M13¹⁶ and recently for the Pf3 protein as well.¹⁷

NMR Structure Calculation

The solution structures of both the PH domain and the ssDBP were calculated by MD-based simulated annealing^{18,19} using a modified version of the X-PLOR program.²⁰ This version is capable of processing ambiguous nuclear Overhauser effect (NOE) data²¹ and was previously used for calculating the refined structure of the PH domain.¹¹ Symmetry restraints previously used for calculating the structure of ssDBP¹² were omitted if not specified otherwise.

The experimental data sets used for structure calculation are very different for the two systems. High-quality distance constraints for ssDBP were determined from isotope-edited 3D spectra (¹⁵N NOESY-HMQC, ¹³C NOESY-HMQC) of a doubly labeled sample. Apart from the dimerization interface, there was virtually no peak overlap, which allowed for tight distance bounds. In total, 1,145 NOE restraints were used, comprising 1,018 intramonomer, 22 intermonomer, and 105 ambiguous NOEs. Seventy-nine J-coupling restraints per monomer were included in the calculation. In the case of the PH domain, only homonuclear data from a 30 ms and a 80 ms NOESY spectrum were used. The merged dataset initially consisted of 1,998 ambiguous and 505 unambiguous distance restraints. Overlapping peaks and spin diffusion necessitated looser calibration. A large part of the NOE peaks was assigned automatically during structure calculation. Several NOEs were discarded automatically during

calculation, as they consistently could not be fulfilled within a rigid structure. As a result, mobility of some regions, e.g., the small helix in the $\beta 3$ – $\beta 4$ loop, might be underestimated in NMR structure ensembles. The final set of restraints consisted of 486 ambiguous and 1,328 unambiguously assigned distance restraints. A detailed account of the assignment scheme is given in Reference 11.

MD Simulation

Two different simulation methods were applied.

Reduced electrostatics, implicit solvent model

For the coverage of nanosecond timescales, a vacuum simulation was performed using X-PLOR²⁰ and the CHARMM19 united atom force field.²² In order to mimic the mechanical effects of a solvent, an implicit solvent model was adopted: surface atoms of the solute were subjected to Langevin dynamics (LD) with a friction coefficient $\beta = 20 \text{ ps}^{-1}$. The solvent exposure was calculated on an atomwise basis and updated in intervals of 0.1 ps. Langevin dynamics served also as a means of maintaining a constant temperature of 303K. Bond lengths were kept at their respective equilibrium values using SHAKE.²³ Dielectric screening—in solvated simulations a feature of the explicit solvent model—was performed via a distance-dependent dielectric constant ($\epsilon = r$) and scaling by a factor 0.3 of the charges on sidechains bearing net charge. In order to reduce truncation artifacts, a switching function over a 5–9 Å range was applied.²⁴

Full electrostatics, explicit solvent model

Solvated simulations were performed using the particle mesh Ewald (PME)²⁵ implementation of the AMBER4.1 package²⁶ and the Cornell et al. force

field.²⁷ For the PH domain, protonation states of the titrable sites were calculated with the UHBD program package.²⁸ Temperature (303K (PH domain) and 298K (ssDBP)) and pressure (1 atm)²⁹ as well as bond lengths²³ were kept constant during the simulations.

The LD method was applied only to the PH domain. Starting from the refined NMR structure,¹¹ a trajectory of 10 ns length (referred to as LD/NMR) was computed, of which the final 9 ns were used for analysis. The PME method was applied to both systems. In the case of the PH domain also, two different starting structures were used. Equilibrated PH domain trajectories of 500 and 700 ps length were calculated using the refined NMR structure¹¹ and the X-ray structure,¹⁵ respectively, as initial configurations (referred to as PME/NMR and PME/X-ray trajectories). The inositol trisphosphate ligand present in the X-ray structure was not included in the simulation. An equilibrated trajectory of 1,050 ps length using the NMR structure¹² as initial configuration was calculated for ssDBP.

Essential Dynamics Analysis

Information about the correlated motion in a series of coordinate frames is contained in the covariance matrix, whose elements are constructed according to:

$$M_{ij} = \langle (x_i - \langle x_i \rangle)(x_j - \langle x_j \rangle) \rangle \quad (1)$$

x_i and x_j run over the x , y , z coordinates of all atoms considered. In this study, only the C_α atoms of the respective system were considered. It was shown that the correlated motions with the largest amplitudes are backbone modes,⁵ which justifies an analysis that is restricted to the C_α atoms, provided the study focuses on the first few eigenvectors. The average in Equation 1 runs over a series of coordinate frames. These may stem from an MD trajectory or from an ensemble of NMR structures. The overall translational and rotational motion is removed prior to the essential dynamics analysis by transforming to center-of-mass coordinates and least-square fitting to a reference coordinate frame minimizing the C_α displacements. For a comparison of essential spaces (see below) the use of the same reference structure for the removal of overall tumbling in all data sets is a prerequisite. Eigenvectors and eigenvalues of the covariance matrix are modes of concerted motions and corresponding amplitudes, respectively. The modes are sorted according to the size of their amplitudes.⁵ The calculation of the covariance matrix and its diagonalization was performed with the WHATIF program package.³⁰ For the comparison of essential spaces, average cumulative square inner

products (ACSIP)^{31,32} were calculated.

$$\text{ACSIP}(k) = (1/D) \sum_{i=1}^D \sum_{j=1}^k (\tilde{v}_i \cdot \tilde{v}_j)^2 \quad (2)$$

\tilde{v}_i , \tilde{v}_j are the normalized eigenvectors of the two sets to be compared and D is the dimension of the essential space. k runs up to $3N$ with N the number of atoms considered for calculating the eigenvectors. Thus, the first D eigenvectors of a reference set i are rebuilt using all eigenvectors of a trial set j . The cumulative square inner products are averaged over the D eigenvectors of set i . Rebuilding is always possible; however, the characteristics of the rebuild curve, i.e., a plot of $\text{ACSIP}(k)$ vs. k , may vary. A straight diagonal line connecting the points ($\text{ACSIP} = 0$, $k = 0$) and ($\text{ACSIP} = 1$, $k = 3N$) corresponds to no correlation between the two sets. In such a case, the first eigenvectors of the reference set are spread out over all eigenvectors of the trial set. The more convex the curve, the more the two essential spaces are related, the D high-amplitude modes of the reference set being predominantly present among the high-amplitude modes of the trial set. On the other hand, a concave curve would indicate that high-amplitude modes of one set are retrieved among the low-amplitude modes of the other set. Only ACSIPs up to an eigenvector index $k = n - 1$ can be considered, if n is the number of coordinate frames in the trial set, since a set of n structures can only define $n - 1$ directions in conformational space. The eigenvectors with higher indices are meaningless and associated with zero amplitudes.

RESULTS

NMR Structure Ensembles

For both systems, two NMR structure ensembles differing in both number of structures and diversity of the structures were analyzed. They represent different subsets of the total of structures generated by the NMR structure calculation protocol. The X-PLOR energies and energy-sorted RMSD plots serve as criteria for the definition of the subsets. The X-PLOR energy is the sum of the potential energies of the force field terms present during the refinement, i.e., bonds, angles, improper dihedrals, van der Waals interactions, and NOE restraints. The sorted energies are shown in Figure 2.

RMSDs are a way of quantifying the increasing spread of structures when higher energy structures are taken into account and may guide the structure selection process.³⁴ An energy-sorted RMSD plot is given in Figure 3.

The plots of the maximum RMSD (thick lines in Fig. 3) correspond to the energy-sorted RMSD plot proposed in Reference 34, with the difference that we plot RMSD values to the average structure rather than pairwise RMSDs.

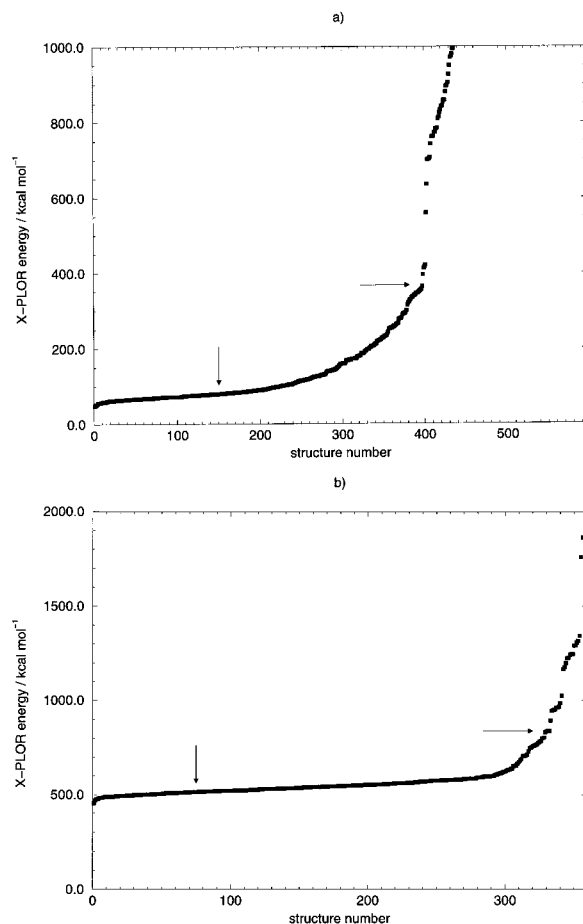


Fig. 2. Sorted X-PLOR energies for 595 PH domain NMR structures (a) and 359 ssDBP NMR structures (b). Only energies below 1,000.0 and 2,000.0 kcal mol⁻¹, respectively, are shown. The lower energies form a continuum (end indicated by the right arrow) that is separated by a gap from the smaller fraction of high-energy structures. The continuum defines set 2 of NMR structures (for details see text). Set 1 in turn is a subset of set 2, i.e., the 150 and 75 lowest energy structures (left arrow), respectively, representing the "standard" result of the refinement procedure.

Structure selection for NMR structure set number 1 (lower diversity) considers the lowest energy structures up to the end of the first marked plateau of the maximum RMSD plot. Similarly, one might choose the first quarter of structures starting from low energies. This yields 150 and 75 structures for the PH domain and ssDBP, respectively, that show similar energies (PH domain: 49.4–79.8 kcal mol⁻¹, ssDBP: 452.6–520.0 kcal mol⁻¹). The energy curve (Fig. 2) then becomes steeper until the continuum ends (PH domain: 364.3 kcal mol⁻¹, ssDBP: 838.6 kcal mol⁻¹). Ensembles with higher diversity (set number 2) comprise all structures with energies below the cutoff criterion defined by the end of continuum. This corresponds to 397 and 332 structures, respectively. Alternatively, one may use the NOE violation energy as a criterion for sorting the

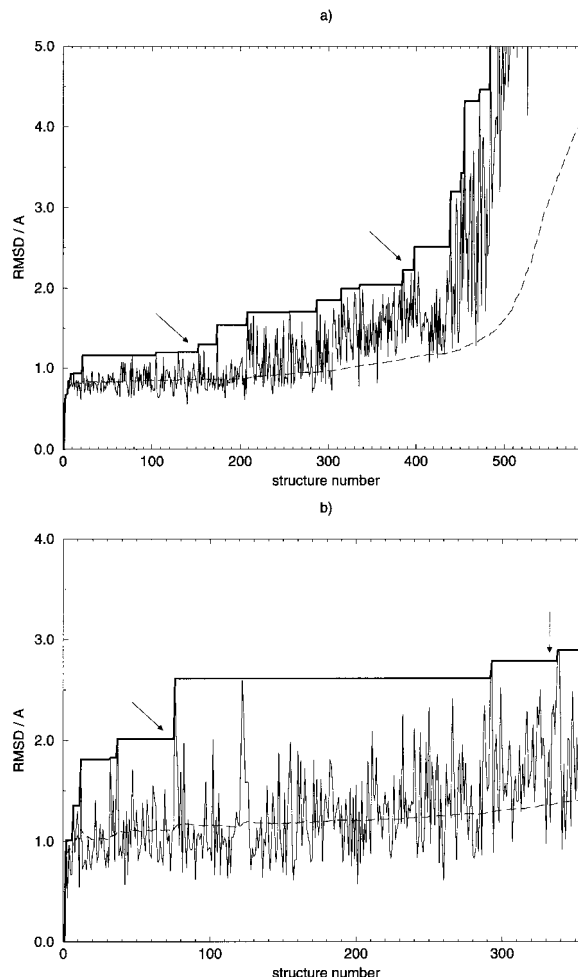


Fig. 3. Energy-sorted RMSD plot for the backbone heavy atoms of the 595 PH domain structures (a) and 359 ssDBP structures (b). The respective comparison structure is the coordinate average of all structures considered so far (coming from low energies), including the current one. Average RMSD from the average structure (dashed line). RMSD averaging also runs over all structures up to the current one. The RMSD of the current structure from the average structure is shown as a thin continuous line; the maximum value assumed by this function as a thick continuous line. The arrows indicate the cutoffs chosen for set 1 and set 2.

structures. Again, a clearly delimited continuum is observed comprising practically the same structures as the total energy continuum and defining a virtually identical essential space (data not shown). The average and the maximum RMSD for the two sets are given in Table I.

In order to make sure that the larger ensembles do not include structures with unacceptable restraint violations, NOEs violated by set 2 but not by set 1 were determined. For the PH domain, 44 restraints are violated by more than 0.3 Å by structures being members of set 2 but not of set 1. Thirty-four of these restraints are NOEs involving nuclei in the β 1– β 2 loop, the β 3– β 4 loop (including the short α -helix) and

TABLE I. Average and Maximum Backbone RMSD Values for the Two NMR Structure Ensembles of the PH Domain and ssDBP

| Ensemble | Average RMSD/Å | Maximum RMSD/Å |
|-----------------|----------------|----------------|
| PH domain set 1 | 0.86 | 1.21 |
| PH domain set 2 | 1.14 | 2.23 |
| ssDBP set 1 | 1.11 | 2.01 |
| ssDBP set 2 | 1.36 | 2.78 |

the $\beta 5$ – $\beta 6$ loop. The long-range NOEs among the remaining ten restraints cluster into one class, i.e., NOEs between the C-terminal end of $\beta 1$ and the N-terminal end of $\beta 7$, the violation of which results from the large-scale mobility of the $\beta 1$ – $\beta 2$ loop. Owing to the high quality of the distance restraints for ssDBP,¹² the resulting energy and energy-sorted RMSD plots show an extended flat region, where both violations and RMSDs do not increase significantly. Only close to the end of the continuum (structures 312 to 332) the refinement energy increases and, concomitantly, the number of violations larger than 0.3 Å. These violations are found predominantly in the DNA binding wing. Thus, the larger ensembles are characterized by enhanced mobility in those regions where the structures are already known to be less well-defined.

Molecular Dynamics Trajectories

The average geometrical properties of the structures generated during the three MD trajectories of the PH domain were determined using the DSSP program.³⁵ A comparison is given in Table II. The solvated trajectories show a larger number of residues in random coil conformation than the Langevin dynamics trajectory. For all trajectories the number is compatible with the low content of secondary structure (55%) of the PH domain. The number of mainchain dihedral angles outside favorable regions of the Ramachandran plot³⁶ is similar for all three trajectories. The radius of gyration is virtually identical for the two solvated trajectories and larger than for the vacuum trajectory, presumably because interaction with the solvent is absent. The PH domain NMR set 2 displays a radius of gyration of 12.82 ± 0.10 Å, which is closer to the solvated simulations than to the vacuum simulation (Table II), indicating that the soft repulsion potential³⁷ used for NMR structure calculation yields structures of appropriate compactness.

For the ssDBP protein, one solvated trajectory was calculated. In Figure 4, RMSDs of the equilibrated trajectory vs. the initial structure and the radius of gyration are given as a function of time.

The average radius of gyration calculated from the trajectory ($R_{\text{gyr}} = 16.72 \pm 0.014$ Å) is very close to the value for NMR set 2 ($R_{\text{gyr}} = 16.78 \pm 0.019$ Å).

Figure 5 compares RMS fluctuations of the C_{α} atoms observed for NMR structures ensembles and MD trajectories of both systems.

The NMR structure ensembles show an overshooting mobility for part of the surface-exposed loops and hairpins, while showing fluctuations smaller than or comparable to the trajectories for the rest of the structures. Similar observations were made for BPTI.³ In the case of the PH domain, there are poor correlations for the fluctuations in the first part of the $\beta 3$ – $\beta 4$ loop (including the short α -helix). Low mobility in the NMR structure ensembles in this region arise from the fact that conflicting NOEs to the helix were omitted during refinement, as they could not be fulfilled simultaneously.

As the MD trajectories serve as a reference for the assessment of the definition of the essential space given by NMR structure ensembles, it is crucial that the essential space definition is sufficiently converged within the trajectories themselves. In Figure 6, subsets of trajectories are compared to the whole trajectories in terms of ACSIP (cf. methods section) curves.

It is evident that subtrajectories approximately half as long as the respective whole trajectories define essential spaces that show very high overlap among themselves and with those defined by the whole trajectories. An almost equally high overlap is observed for subtrajectories of the PME/NMR trajectory of the PH domain (data not shown).

Comparison of Essential Spaces

Essential spaces were compared by average cumulative square inner products (ACSIP; see Methods) of their respective eigenvectors. The dimension of the essential space D was set to 5. This collects approximately 50% of the total mobility inherent in the datasets. A value of 10 for D yields very similar ACSIP data (not shown). The ACSIP curves in Figures 7 and 8 show to what extent the first five modes of the respective reference set are present, predominantly among the low-index modes of the trial sets. The more this is the case, the more the curves are convex. A straight diagonal would correspond to no correlation at all. The comparison is meaningful only for the first $n - 1$ eigenvectors, if n is the number of structures in the smaller dataset (150 (PH domain) and 75 (ssDBP)) (cf. Methods).

In the case of the PH domain, the first 9.4% of eigenvectors of NMR set 2 contain on average 50% of the first five eigenvectors of the PME/NMR trajectory (Fig. 7a). Qualitatively, the MD trajectories of the PH domain are as distant from each other as the MD trajectories from the NMR set 2. (Quantitative analysis reveals that the comparison simulations done on the PH domain perform slightly better than the NMR-derived set of eigenvectors: 6.3% of the eigenvectors of both the LD/NMR and the PME/X-ray trajectory are sufficient for rebuilding 50% of the

TABLE II. Average Geometrical Properties of the Structures Generated During the MD Trajectories of the PH Domain

| | Φ, Ψ | random coil | H-bonds | $R_{\text{gyr}}/\text{\AA}$ |
|-----------|-----------------|----------------|-----------------|-----------------------------|
| PME/X-ray | 8.77 ± 2.20 | 36.9 ± 3.9 | 101.0 ± 3.5 | 13.05 ± 0.13 |
| PME/NMR | 7.08 ± 2.03 | 38.4 ± 3.3 | 101.1 ± 4.4 | 13.06 ± 0.12 |
| LD/NMR | 7.52 ± 1.53 | 21.1 ± 3.0 | 96.2 ± 4.0 | 12.10 ± 0.05 |

Φ, Ψ /number of mainchain dihedral angles in unfavorable regions of the Ramachandran plot; random coil/number of residues (out of 106) in random coil conformation; H-bonds/backbone-backbone hydrogen bonds; R_{gyr} /radius of gyration.

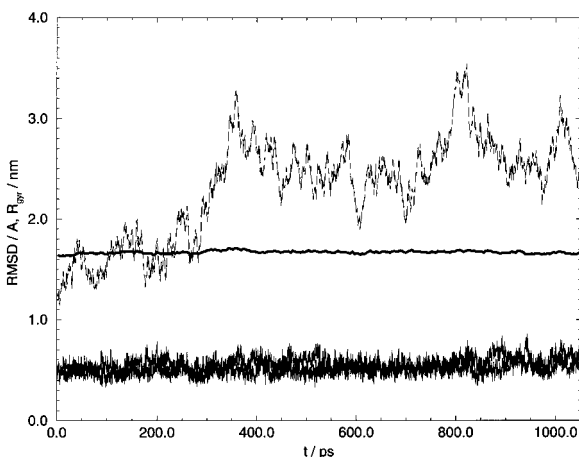


Fig. 4. Radius of gyration (thick continuous line) and RMSD of all C_{α} atoms (dashed line) of the ssDBP protein vs. the starting NMR structure as a function of time. The RMSD of the C_{α} atoms in the five-stranded β -sheet vs. the starting structure were determined individually for each chain, yielding two very similar plots (thin continuous lines at the bottom). Thus, the core of each monomer is very stable throughout the trajectory.

first five eigenvectors of the PME/NMR trajectory). In the case of the ssDBP protein, four eigenvectors (corresponding to less than 1%) of NMR set 2 are sufficient (Fig. 8a). NMR- and MD-derived modes are here less distant than MD-derived modes for different trajectories of the PH domain.

Instead of using the MD-derived essential space as a reference, the NMR ensemble-derived set of eigenvectors may be used. The three MD comparison simulations performed on the PH domain yield very similar ACSIP curves (Fig. 7b). For ssDBP, the high overlap is seen in both directions, i.e., independent of the choice of the reference set (Fig. 8b).

The difference between NMR sets 1 and 2 with regard to ACSIPs is not pronounced, although NMR set 2 always performed better. This results predominantly from the increased number of structures in set 2, which allows a statistically more significant definition of covariances. A more pronounced difference between the two sets are the amplitudes of motion.

The comparison of large-scale correlated motion in terms of average cumulative square inner products deals with normalized eigenvectors that are ordered

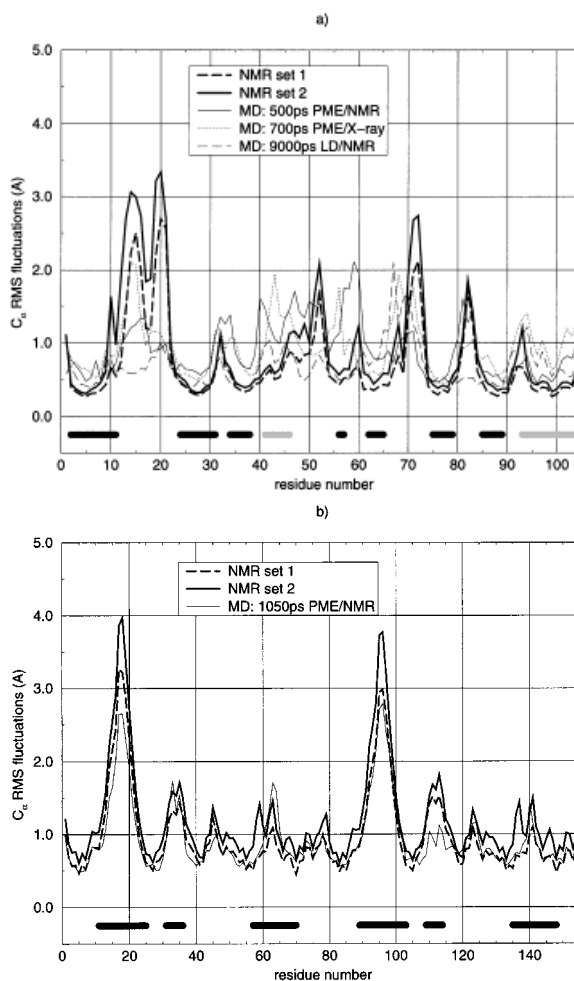


Fig. 5. C_{α} RMS fluctuations calculated from NMR structure ensembles and MD trajectories. (a) PH domain. The bars indicate the elements of secondary structure (black/ β -strands, gray/ α -helices). (b) ssDBP. Bars indicate the DNA binding wings, the complex loops, and the dyad loops.

according to their associated amplitudes. However, the actual values of these amplitudes, which are the eigenvalues of the covariance matrix, are not considered. In Figure 9 an eigenvalue comparison for the PH domain NMR structure sets and MD trajectories is given. Differing from MD results, the NMR-derived modes show a less steep amplitude distribu-

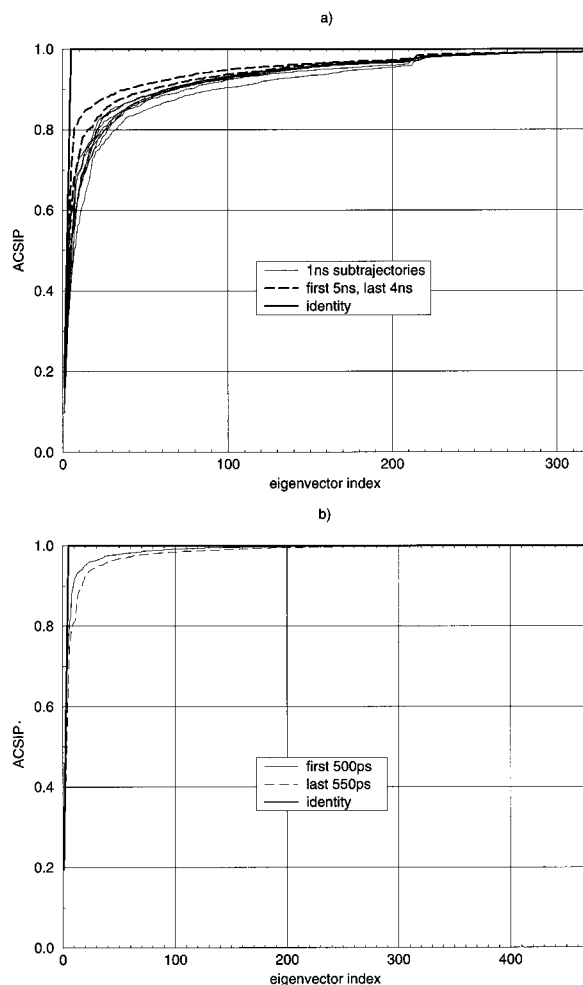


Fig. 6. Comparison of subsets of trajectories to whole trajectories in terms of average cumulative square inner products. (a) Langevin dynamics trajectory of the PH domain, (b) solvated simulation of the ssDBP protein. "Identity" refers to the self-comparison.

tion. Thus, separation between "essential modes" and the remainder is less pronounced. Mobility is spread out over more modes.

Resulting from the compactness of the PH domain structure in the LD simulation (Table II), its mobility is highly restricted in comparison to the solvated simulations.

The amplitudes given in Figure 9 are associated with different sets of eigenvectors, i.e., they are not strictly comparable; rather, they give a global view of the scale of fluctuations. A more strict comparison is feasible in the case of the ssDBP protein, as the essential spaces defined by NMR structure ensembles and MD simulation match very closely. In Figure 10, the RMS displacements of NMR sets 1 and 2 from the respective mean structure along the eigenvectors defined by the 1,050 ps solvated simulation are shown. Thus, only one single set of modes underlies the comparison. The corresponding RMS

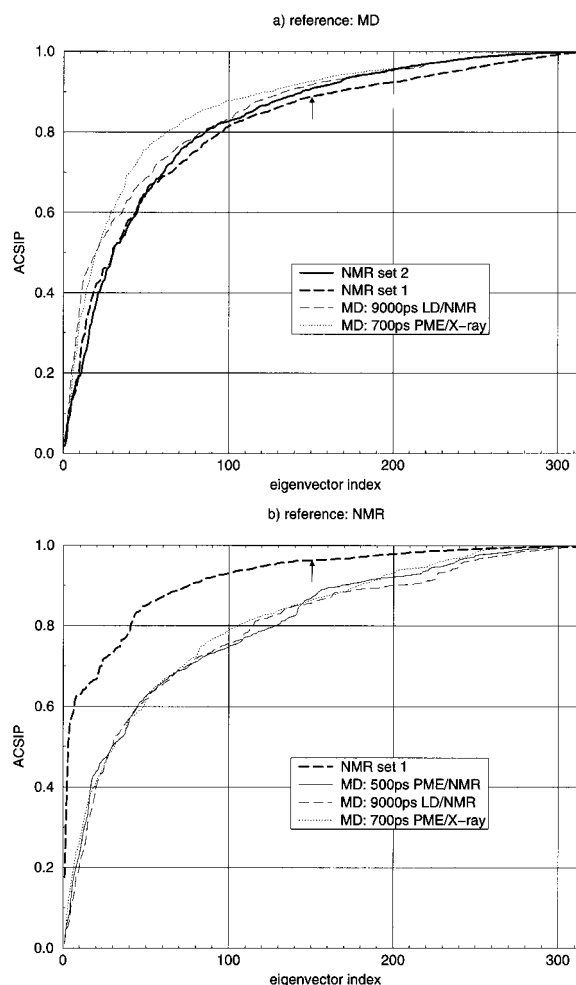


Fig. 7. Comparison of essential spaces of the PH domain by ACSIP. The cumulative square inner product is the sum of square projections of a particular eigenvector of one set (reference set) on the whole series of eigenvectors of a second set (trial set). Arrows indicate the last eigenvector with nonzero amplitude for the respective dataset. The reference set comprises the first five eigenvectors obtained from a 500 ps solvated simulation of the PH domain (PME/NMR) (a) and from set 2 of NMR structures (b), respectively. (a) Set 2 is only slightly worse in spanning the essential space than two comparison simulations. (b) Using set 2 of NMR structures as the reference, the three MD simulations perform rather similarly.

displacements occurring during the trajectory itself are square roots of the eigenvalues of the covariance matrix and are included for comparison. NMR set 2 reproduces very well the amplitude associated with the motion along the first eigenvector obtained from MD simulation, but overestimates the amplitudes of the second and the third essential mode.

Influence of Restraint Specification on the Essential Subspace

Two questions connected to the definition of restraints used in NMR structure refinement were addressed. First, the distance bounds of the flat-

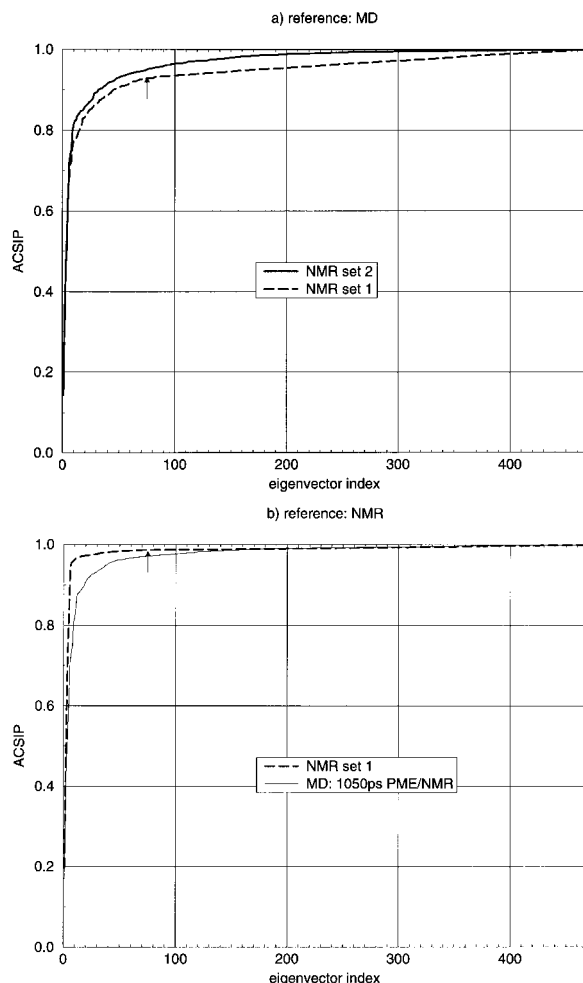


Fig. 8. Comparison of essential spaces for the Pf3 ssDBP protein. Arrows indicate the last eigenvector with nonzero amplitude for the respective dataset. (a) Reference: 1,050 ps solvated MD simulation; (b) reference: NMR set 2. The overlap of essential spaces is extraordinarily high.

bottom part of NOE restraint potential were changed and their influence on the description of the essential space was monitored. Second, the influence of symmetry restraints commonly used for the refinement of structures showing internal symmetry was studied for ssDBP, which contains two C_2 symmetry-related monomers.

Two modified datasets were generated by widening the bounds (reducing lower bounds and increasing upper bounds) by 1 and 2 Å. In each case, 200 structures were calculated. The energy profile remains essentially the same (data not shown) as for the original bounds (Fig. 2a). The energy-sorted RMSD plots change significantly, owing to the increasing spread of structures when distance restraints are loosened (cf. Fig. 11). At the same time, the convergence rate drops (Fig. 11a), as does the quality of the structures as measured by the RMSD from the X-ray structure (Fig. 11b).

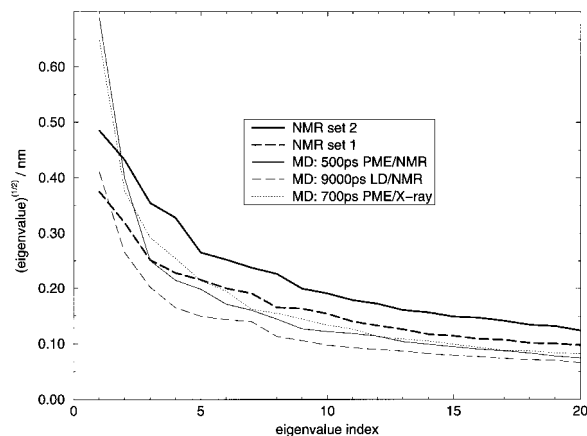


Fig. 9. Sorted amplitudes (square roots of eigenvalues) of the respective first 20 essential modes of PH domain NMR structure ensembles and MD trajectories. Set 2 of NMR structures displays larger amplitudes than set 1 throughout. The two solvated simulations display markedly larger amplitudes of the respective first essential mode than both the NMR structure families and the vacuum simulation.

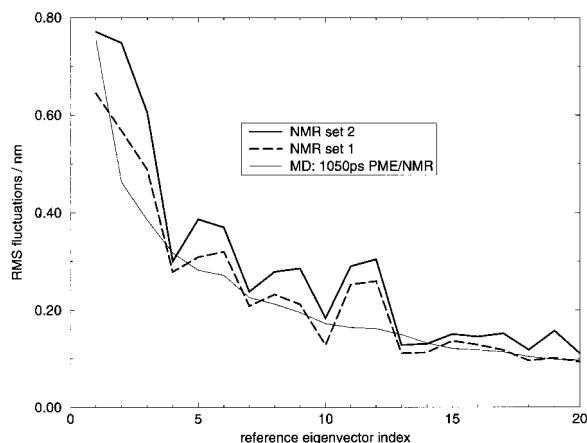


Fig. 10. Amplitudes obtained by cross-projections: NMR sets 1 and 2 and the 1,050 ps PME/NMR trajectory of the ssDBP protein are projected along the eigenvectors defined by the trajectory. For the trajectory, the RMS fluctuations along eigenvectors are equivalent to the square roots of the eigenvalues of the covariance matrix.

The ACSIP of the eigenvectors defined by the respective NMR structure ensembles (132 and 109 structures, respectively) with the first five eigenvectors from the 500 ps PME/NMR trajectory is only slightly affected by loosened distance bounds (Fig. 12a). The ACSIP curves for distance bounds looser by 1 Å are steeper below 0.5, but run below the curve for the original bounds beyond 0.5. Further loosening the bounds by adding 2 Å to the original bounds has no significant effect.

Plots of amplitudes of all datasets with looser bounds run throughout above all plots in Figure 9 (cf. Fig. 12b). Thus, the 50 lowest-energy structures calculated with bounds loosened by 1 Å overestimate mobility.

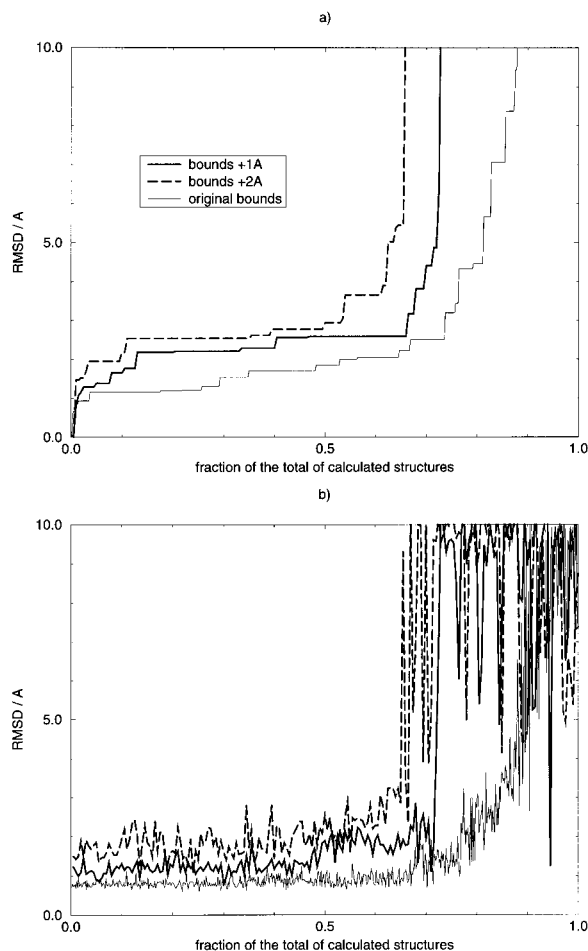


Fig. 11. Influence of looser distance bounds on diversity and quality of structures (PH domain). The total number of structures is 595 for the original bounds and 200 for the two calculations using widened bounds, respectively. (a) Maximum backbone RMSD from the average structure (cf. Fig. 3). (b) RMSD of the backbone of secondary structure elements versus the crystal structure.¹⁵

The influence of symmetry restraints in the refinement of the dimeric ssDBP protein is dramatic. It was analyzed using an ensemble of 80 structures calculated with symmetry restraints (referred to as NMR/sym). The RMSD between the two monomers was minimized using noncrystallographic symmetry (NCS) restraints and artificial distance restraints were invoked in order to enforce the C_2 symmetry.^{38,12} The high overlap with the essential space defined by the trajectory breaks down when C_2 symmetry is enforced (cf. Fig. 13).

The overlap with the first five eigenvectors defined by NMR set 2 of ssDBP structures is equally bad (data not shown). The low number of structures in this ensemble does not explain the bad performance (cf. Fig. 8, where NMR set 1 holding 75 structures yields excellent overlap). The low number of structures gives rise to a loss of correlation in the ACSIP curves beyond the eigenvector index that equals the

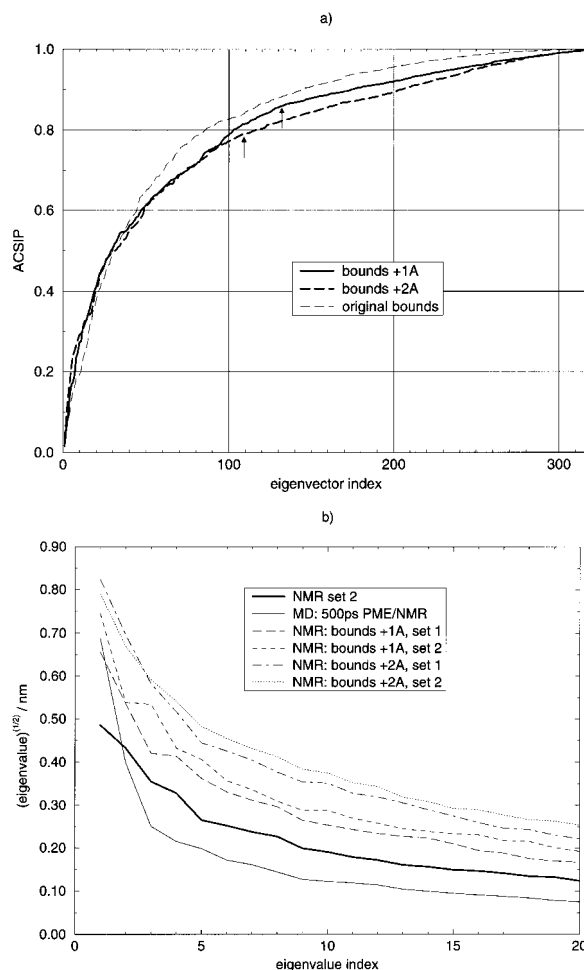


Fig. 12. Influence of distance bounds on modes and amplitudes (PH domain). (a) Essential space overlap with the PME/NMR trajectory. Arrows indicate the last eigenvector with nonzero amplitude for the respective dataset. (b) Amplitudes.

number of structures used. This is apparent from the straight ACSIP line beyond eigenvector 80 in Figure 13. Really critical, however, is the low ACSIP reached by the first 79 eigenvectors. In order to track down the reason for the marked influence of symmetry restraints in refinement, the type of motion described by the respective eigenvectors was inspected. In Figure 14, the components of the first five eigenvectors of the trajectory and the ensemble calculated with symmetry restraints are shown. For each C_α atom i the value of $\sqrt{x_i^2 + y_i^2 + z_i^2}$ is given, where (x_i, y_i, z_i) are the (x, y, z) components for atom i in the respective eigenvector. The plots indicate where the motion associated with a particular eigenvector is located along the sequence of the protein.

The trajectory is characterized by two features that are virtually absent from the NMR structure ensemble calculated using symmetry restraints: (1) There is asymmetry in the motion sampled by the trajectory. This is obvious from the plots of the

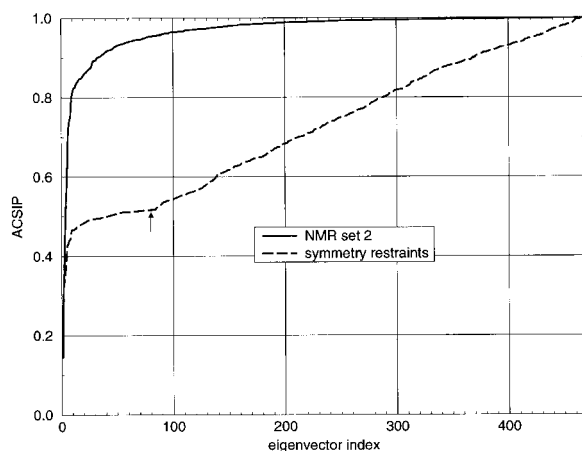


Fig. 13. Influence of symmetry restraints on the definition of essential space (ssDBP). The arrow indicates the last eigenvector with nonzero amplitude for the respective dataset.

components of all five eigenvectors shown. Correlations and component sizes of one chain are not retrieved in the component pattern for the other chain. Exactly the latter is enforced, however, by symmetry restraints. (2) There are nontrivial dynamic cross-correlations, i.e., correlations between structural elements residing at a distance from each other. Part of these are retrieved in the NMR/sym ensemble, i.e., those that are enforced by the restraints, e.g., between equivalent stretches of the two chains. Other nontrivial dynamic cross-correlations, as between the DNA binding wing and the complex loop within one monomer, are absent or present but much weaker in the NMR/sym ensemble.

DISCUSSION

Ensemble refinement³⁹ was put forward as a method that accounts for the mobility inherent in NOE data. The distance averages over a small ensemble of structures (typically two copies of the molecule) are fitted to the distance restraints. By contrast, the ensembles studied in this work are generated by restraining each individual structure to the experimental distance data. Ensemble refinement proved particularly successful in cases where conflicting NOEs cannot be fulfilled simultaneously by single structures. It is computationally less expensive than refinement using time-averaged restraints,^{40,41} which has the further drawback of generating an uneven temperature distribution in the system.⁴¹ Unfortunately, very small ensembles of only two copies sometimes contain too many degrees of freedom and show too-divergent behavior.³⁹ Furthermore, we note that a subset of restraints (torsion angles, hydrogen bonds) is not allowed to average.³⁹ In this study, instead of using an enhanced refinement protocol the diversity of structures obtained from the "standard" protocol was examined for mobil-

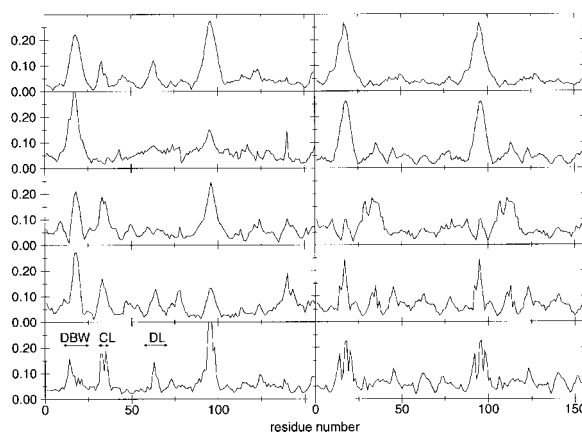


Fig. 14. Eigenvector components for the first five eigenvectors (from top to bottom) of the 1,050 ps trajectory (left column) and the NMR structure ensemble calculated using symmetry restraints (right column). The first monomer consists of residues 1–78, the second of residues 79–156. Residue ranges comprising the DNA binding wing (DBW, residues 11–25), the complex loop (CL, residues 31–36), and the dyad loop (DL, residues 57–70) of monomer 1 are indicated in the bottom left plot.

ity information. Thus, each refined structure was interpreted as a conformational substate of a real ensemble.

MD simulations are the only source of sufficiently detailed dynamics information for the comparison of collective motion pursued in this study. Their use as a reference, however, requires further justification. The interaction model used for the generation of the reference trajectories combines a state-of-the-art all-atom force field²⁷ with a consistent description of the electrostatic interaction.²⁵ We note the very stable behavior of the central five-stranded β -sheet in both monomers of ssDBP throughout the trajectory. The accuracy of the comparison may be estimated in the case of the PH domain, where the essential space definitions given by three different trajectories employing two different methods are as close to each other as they are to the NMR structure bundle. This indicates also a certain robustness of correlated motion toward the simulation method reported previously.³¹ The simulated mainchain flexibility of ssDBP is supported by ¹⁵N relaxation measurements.¹⁷ The high overlap of the essential spaces of subtrajectories with those of the respective entire trajectories indicates a high degree of convergence.

The similarity of large-scale correlated motion found in this comparison of NMR structure ensembles and MD trajectories is surprising because MD simulation and NMR structure calculation employ both different protocols and different potential functions. Long-range electrostatic interactions are completely absent during NMR structure calculation. Nevertheless, large-scale correlated fluctuations are accessible to the proteins also in the

simplified energy landscape defined by the chemical force field used for NMR refinement and the restraints. It appears that the actual direction of these fluctuations in conformational space is sufficiently guided and confined by the experimental restraints, thus yielding correlated fluctuations similar to those observed in MD trajectories. The density of long-range NOEs is lower for atoms in the surface loops of the PH domain and the DNA binding wings of the ssDBP protein than for other parts of the molecules. As these parts of the structures are involved in high-amplitude motions in simulation, in part the overlap may arise from the fact that low NOE density coincides with true mobility in case of the two systems considered, which is supported by ^{15}N relaxation experiments on ssDBP.¹⁷ Still, the observation that nontrivial dynamic cross-correlations, as between the DNA binding wing and the complex loop in ssDBP, are retrieved in the NMR ensembles cannot be explained by this simple reasoning. Retrieving this type of correlated motion is more than just detecting regions with the largest mobility. The high overlap of essential spaces appears to offer a fast route to an approximate description of correlated motion, considering that NMR structure ensembles are calculated in a much shorter time than a nanosecond solvated MD trajectory.

The comparison of amplitudes reveals that the commonly reported NMR structure ensembles containing only low energy structures that fulfill the restraints to a high extent do not reproduce the amplitudes of motion observed in the MD trajectories. A related observation was made for simulations using time-averaged distance restraints,¹³ which represent less stringent restraints than the static distance restraints used in standard structure calculation. Furthermore, it was shown that correlations between the global backbone RMSD per residue and the squared order parameters of backbone ^{15}N -H vectors for ribonuclease T₁ arise only upon inclusion of higher-energy structures (cf. Fig. 3 in Ref. 1). One may think of two means of increasing the conformational sampling of an NMR structure ensemble. One is including higher-energy structures, the other uses loosened distance bounds. In the present study, although a close agreement of amplitudes of all essential modes is not achieved, a better matching of amplitudes between MD trajectories and NMR structure ensembles is observed if the latter include higher-energy structures. This simultaneously improves the overlap with the essential space defined by the MD simulation. We therefore suggest the end of the continuum of the total potential energies (or—with equivalent effect—of the NOE violation energies) as a new cutoff criterion for structure selection, if an ensemble is desired that correlates with an MD-based definition of amplitudes of large-scale correlated motion. This corresponds to maximum backbone RMSDs from the average structure

between 2 and 3 Å for the two systems considered here. Violations present in the wider bundle, but not in the tighter one, are predominantly located in those parts of the structures that are less well-defined in the tight bundle.

The influence of symmetry restraints for the refinement of structures with internal symmetry was investigated in the case of ssDBP. Although symmetry restraints are necessary when ambiguities are present in the NOE restraints,³⁸ they turned out to impair the sampling of conformational space by enforcing symmetric structures. Snapshots of symmetric multimers are not necessarily symmetric, even if on average symmetry is conserved.⁴² Hence, if dynamic information is to be obtained from an ensemble of symmetric multimers, we suggest to calculate an additional ensemble without symmetry restraints.

Looser distance restraints, being an alternative means of obtaining enhanced mobility instead of wider bundles, turned out to have negligible effects on the definition of essential space. At the same time, mobility is overestimated very easily and the quality of structures as measured by the RMSD of the secondary structure from the X-ray structure declines when bounds are loosened. We think that the use of wider structure bundles, including higher-energy structures—which one gets for free—is both a faster and more consistent way of obtaining dynamics information.

ACKNOWLEDGMENTS

The authors thank Daan van Aalten for stimulating discussions about the essential dynamics analysis and Rob Hooft and Gert Vriend for the excellent support with the WHATIF package. R.A. acknowledges an Erwin-Schrödinger fellowship (project number J01261-CHE) of the Austrian Science Foundation (FWF).

REFERENCES

1. Pfeiffer, S., Karimi-Nejad, Y., Rüterjans, H. Limits of NMR structure determination using variable target function calculations: Ribonuclease T₁, a case study. *J. Mol. Biol.* 266:400–423, 1997.
2. Koning, T.M.G., Boelens, R., van der Marel, G.A., van Boom, J.H., Kaptein, R. Structure determination of a DNA octamer in solution by NMR spectroscopy. Effect of fast local motions. *Biochemistry* 30:3787–3797, 1991.
3. Berndt, K.D., Güntert, P., Wüthrich, K. Conformational sampling by NMR solution structures calculated with the program DIANA evaluated by comparison with long-time molecular dynamics calculations in explicit water. *Proteins* 24:304–313, 1996.
4. Berendsen, H.J.C. Bio-molecular dynamics comes of age. *Science* 271:954–955, 1996.
5. Amadei, A., Linssen, A.B.M., Berendsen, H.J.C. Essential dynamics of proteins. *Proteins* 17:412–425, 1993.
6. Ichiye, T., Karplus, M. Collective motions in proteins: A covariance analysis of atomic fluctuations in molecular dynamics and normal mode simulations. *Proteins* 11:205–217, 1991.

7. van der Spoel, D., de Groot, B., Hayward, S., Berendsen, H.J.C., Vogel, H.J. Bending of the calmodulin central helix: A theoretical study. *Protein Sci.* 5:2044–2053, 1996.
8. van Aalten, D.M.F., Amadei, A., Bywater, R., Findlay, J.B.C., Berendsen, H.J.C., Sander, C., Stouten, P.F.W. A comparison of structural and dynamic properties of different simulation methods applied to SH3. *Biophys. J.* 70:684–692, 1996.
9. van Aalten, D.M.F., Jones, P.C., de Sousa, M., Findlay, J.B.C. Engineering protein mechanics: Inhibition of concerted motions of the cellular retinol binding protein by site-directed mutagenesis. *Protein Eng.* 10:31–37, 1997.
10. Macias, M.J., Musacchio, A., Ponstingl, H., Nilges, M., Saraste, M., Oschkinat, H. Structure of the pleckstrin homology domain from β -spectrin. *Nature* 369:675–677, 1994.
11. Nilges, M., Macias, M., O'Donoghue, S.I., Oschkinat, H. Automated NOESY interpretation with ambiguous distance restraints: The refined NMR solution structure of the pleckstrin homology domain from β -spectrin. *J. Mol. Biol.* 269:408–422, 1997.
12. Folmer, R.H.A., Nilges, M., Konings, R.N.H., Hilbers, C.W. Solution structure of the single-stranded DNA binding protein of the filamentous *Pseudomonas* phage Pf3: Similarity to other proteins binding to single-stranded nucleic acids. *EMBO J.* 14:4132–4142, 1995.
13. Scheek, R.M., van Nuland, N.A.J., de Groot, B.L., Amadei, A. Structure from NMR and molecular dynamics: Distance restraining inhibits motion in the essential subspace. *J. Biomol. NMR* 5:106–111, 1995.
14. Feher, V.A., Baldwin, E.P., Dahlquist, F.W. Access of ligands to cavities within the core of a protein is rapid. *Nat. Struct. Biol.* 3:516–521, 1996.
15. Hyvönen, M., Macias, M.J., Nilges, M., Oschkinat, H., Saraste, M., Wilmanns, M. Structure of the binding site for inositol phosphates in a PH domain. *EMBO J.* 14:4676–4685, 1995.
16. Folmer, R.H.A., Nilges, M., Folkers, P.J.M., Konings, R.N.H., Hilbers, C.W. A model of the complex between single-stranded DNA and the single-stranded DNA binding protein encoded by gene V of filamentous bacteriophage M13. *J. Mol. Biol.* 240:341–357, 1994.
17. Folmer, R.H.A., Nilges, M., Papavoine, C.H.M., Harmsen, B.J.M., Konings, R.N.H., Hilbers, C.W. Refined structure, DNA binding studies, and dynamics of the bacteriophage Pf3 encoded single-stranded DNA binding protein. *Biochemistry* 36:9120–9135, 1997.
18. Nilges, M., Gronenborn, A.M., Brünger, A.T., Clore, G.M. Determination of three-dimensional structures of proteins by simulated annealing with interproton distance restraints: Application to crambin, potato carboxypeptidase inhibitor and barley serine protease inhibitor 2. *Protein Eng.* 2:27–38, 1988.
19. Nilges, M., Kuszewski, J., Brünger, A.T. Sampling properties of simulated annealing and distance geometry. In: Hoch, J.C., Poulsen, F.M., Redfield, C. (eds). "Computational Aspects of the Study of Biological Macromolecules by Nuclear Magnetic Resonance Spectroscopy." New York: Plenum Press, 1991:451–455.
20. Brünger, A. "X-PLOR: A System for X-ray Crystallography and NMR." New Haven: Yale University Press, 1992.
21. Nilges, M. Calculation of protein structures with ambiguous distance restraints. Automated assignment of ambiguous NOE crosspeaks and disulphide connectivities. *J. Mol. Biol.* 245:645–660, 1995.
22. Brooks, B.R., Brucoleri, R.E., Olafson, B.D., States, D.J., Swaminathan, S., Karplus, M. CHARMM: A program for macromolecular energy, minimization, and dynamics calculations. *J. Comp. Chem.* 4:187–217, 1983.
23. van Gunsteren, W.F., Berendsen, H.J.C. Algorithms for macromolecular dynamics and constraint dynamics. *Mol. Phys.* 34:1311–1327, 1977.
24. Loncharich, R.J., Brooks, B.R. The effects of truncating long-range forces on protein dynamics. *Proteins* 6:32–45, 1989.
25. Darden, T., York, D., Pedersen, L. Particle mesh Ewald: An $N\log(N)$ method for Ewald sums in large systems. *J. Chem. Phys.* 98:10089–10092, 1993.
26. Pearlman, D.A., Case, D.A., Caldwell, J.W., Ross, W.S., Cheatham, T.E. III, Ferguson, D.M., Seibel, G.L., Chandra Singh, U., Weiner, P.K., Kollman, P.A. AMBER 4.1. San Francisco: University of California, 1995.
27. Cornell, W.D., Cieplak, P., Bayly, C.I., Gould, I.R., Merz, K.M. Jr., Ferguson, D.M., Spellmeyer, D.C., Fox, T., Caldwell, J.W., Kollman, P.A. A second generation force field for the simulation of proteins, nucleic acids, and organic molecules. *J. Am. Chem. Soc.* 117:5179–5197, 1995.
28. Madura, J.D., Briggs, J.M., Wade, R.C., Davis, M.E., Luty, B.A., Ilin, A., Antosiewicz, J., Gilson, M.K., Bagheri, B., Scott, L.R., McCammon, J.A. Electrostatics and diffusion in solution: Simulations with the University of Houston Brownian dynamics program. *Comp. Phys. Comm.* 91:57–85, 1995.
29. Berendsen, H.J.C., Postma, J.P.M., DiNola, A., Haak, J.R. Molecular dynamics with coupling to an external bath. *J. Chem. Phys.* 81:3684–3690, 1984.
30. Vriend, G. WHATIF: A molecular modelling and drug design program. *J. Mol. Graph.* 8:52–56, 1990.
31. de Groot, B.L., van Aalten, D.M.F., Amadei, A., Berendsen, H.J.C. The consistency of large concerted motions in proteins in molecular dynamics simulations. *Biophys. J.* 71:1707–1713, 1996.
32. van Aalten, D.M.F., de Groot, B.L., Findlay, J.B.C., Berendsen, H.J.C., Amadei, A. A comparison of techniques for calculating protein essential dynamics. *J. Comp. Chem.* 18:169–181, 1997.
33. Kraulis, P.J. MOLSCRIPT: A program to produce both detailed and schematic plots of protein structures. *J. Appl. Crystallogr.* 24:946–950, 1991.
34. Widmer, H., Widmer, A., Braun, W. Extensive distance geometry calculations with different NOE calibrations: New criteria for structure selection applied to Sandostatin and BPTI. *J. Biomol. NMR* 3:307–324, 1993.
35. Kabsch, W., Sander, C. Dictionary of protein secondary structure: Pattern recognition of hydrogen-bonded and geometrical features. *Biopolymers* 22:2577–2637, 1983.
36. Ramachandran, G.N., Ramakrishnan, C., Sasisekharan, V. Stereochemistry of polypeptide chain configurations. *J. Mol. Biol.* 7:95–99, 1963.
37. Nilges, M., Clore, G.M., Gronenborn, A.M. Determination of three-dimensional structures of proteins by hybrid distance geometry-dynamical simulated annealing calculations. *FEBS Lett.* 229:317–324, 1988.
38. Nilges, M. A calculation strategy for the structure determination of symmetric dimers by ^1H NMR. *Proteins* 17:297–309, 1993.
39. Bonvin, A.M.J.J., Brünger, A.T. Conformational variability of solution nuclear magnetic resonance structures. *J. Mol. Biol.* 250:80–93, 1995.
40. Torda, A.E., Scheek, R.M., van Gunsteren, W.F. Time-dependent distance restraints in molecular dynamics simulation. *Chem. Phys. Lett.* 157:289–294, 1989.
41. Torda, A.E., Scheek, R.M., van Gunsteren, W.F. Time-averaged nuclear Overhauser effect distance restraints applied to tendamistat. *J. Mol. Biol.* 214:223–235, 1990.
42. Chillemi, G., Falconi, M., Amadei, A., Zimatore, G., Desideri, A., Di Nola, A. The essential dynamics of Cu, Zn superoxide dismutase: Suggestion of intersubunit communication. *Biophys. J.* 73:1007–1018, 1997.